The age of Wolfe Creek Meteorite Crater (*Kandimalal*), Western Australia

Timothy T. Barrows*

School of Earth and Environmental Sciences, University of Wollongong, Wollongong, NSW, 2522, Australia and

Department of Geography, University of Portsmouth, Portsmouth, PO1 2UP, UK

John Magee

Research School of Earth Sciences, Australian National University, ACT 0200, Australia

Gifford Miller

INSTAAR and Department of Geological Sciences, University of Colorado, Boulder CO 80309 USA

L. Keith Fifield

Department of Nuclear Physics, Research School of Physics and Engineering, The Australian National University, Canberra, ACT 2601 Australia

In press in *Meteoritics and Planetary Science*

*Corresponding author's contact details:

Prof. Tim Barrows

Email: Tim.Barrows@uow.edu.au

ABSTRACT

Wolfe Creek Crater lies in northwestern Australia at the edge of the Great Sandy Desert. Together with Meteor Crater, it is one of the two largest craters on Earth from which meteorite fragments have been recovered. The age of the impact is poorly constrained and unpublished data places the event at about 300,000 years ago. In comparison, Meteor Crater is well constrained by exposure dating. In this paper we present new ages for Wolfe Creek Crater from exposure dating using the cosmogenic nuclides ^{10}Be and ^{26}Al, together with optically stimulated ages (OSL) on sand from a site created by the impact. We also present a new topographic survey of the crater using photogrammetry. The exposure ages range from ~86-128 ka. The OSL ages indicate the age of the impact is most likely to be ~120 ka with a maximum age of 137 ka. Considering the geomorphic setting, the most likely age of the crater is 120 ± 9 ka. Lastly, we review the age of Meteor Crater in Arizona. Changes in production rates and scaling factors since the original dating work revise the impact age to 61.1 ± 4.8 ka, or ~20% older than previously reported.

INTRODUCTION

The Earth is continually bombarded by meteors and the largest of these leave significant geomorphic traces as impact craters. Wolfe Creek Meteorite Crater (*Kandimalal* in Djaru language) is one of the largest meteorite impacts on Earth within the last million years. Together with Meteor (Barringer) Crater, it is one of the two best preserved large, simple impact craters from which meteorite fragments have been recovered. The crater is situated 820 km southwest of Darwin in Western Australia. The crater was created by a meteorite about 15 m in diameter (~14 kt) at an impact incidence of 45 – 30° from a northeasterly direction, travelling at 17 $km.s^{-1}$ with energy of impact of about 0.54 Mt of TNT (O'Neill and Heine, 2005; Shoemaker et al., 2005). The meteorite is structurally a medium octahedrite with 8.6-9.22% Ni (Buchwald, 1975; Taylor, 1965) and belongs to chemical group IIIAB (Scott et al., 1973).

Hawke (2003) and O'Neill and Heine (2005) conducted ground-based geophysical surveys on the crater and found the crater has a relatively simple structure with the crater floor predicted to be 120-150 m beneath the present surface. Despite the size of the crater, it is estimated that the impact was only associated with about 800 m^3 of melt (O'Neill and Heine, 2005). The projectile would have shock-melted, mixed with up to an order of magnitude greater volume of local bedrock melt and splashed as an ejecta blanket. Ejecta from the crater covers much of the outer crater rim (O'Neill and Heine, 2005) and includes 'shale balls', a mixture of the original Fe-Ni meteorite and bedrock (LaPaz, 1954). Approximately1000 kg of "iron shale" was collected from the southwest sector of the crater rim (Fudali, 1979).

Early estimates of the age of Wolfe Creek Crater identified it as less than 2 million years old (McNamara, 1982). Shoemaker et al. (1990) reported unpublished data giving two age

estimates. The first was the terrestrial age based on decay ratios of $^{36}Cl/^{10}Be$ and $^{41}Ca/^{36}Cl$ on a meteorite giving an age of about 300 ka. The second was from ^{10}Be and ^{26}Al exposure ages from the wall of the crater which gave ages of ~30 ka. Meteor Crater was dated at approximately the same time and produced younger exposure ages of 49.2 ± 1.7 (Nishiizumi et al., 1991) and 49.7 ± 0.85 years (Phillips et al., 1991). The only other large impact crater that has been exposure dated is Lonar Crater in India with a likely age of 37.5 ± 5.0 ka (Nakamura et al., 2014).

In this paper we re-examine the geomorphology of Wolfe Creek Crater and review the age of the impact. To explore the geomorphology of the crater we constructed a 3D model of it using photogrammetry. Second, we present direct exposure ages for ejecta on the crater rim exposed during the impact and limiting luminescence ages for the formation of a sand dune after the impact. Additionally, we review the age of Meteor Crater. Based on the revision of the age of Wolfe Creek Crater, we provide a new estimate for the cratering rate in Australia for the last ~10^5 years.

GEOMORPHOLOGY

Wolfe Creek Crater is situated on the edge of the Great Sandy Desert dune field which is dominated by ENE-WSW trending longitudinal dunes spaced ~1 km apart, with basal widths of about 100 m (Miller et al., 2018). The formation of the crater perturbed the surface wind-field and consequent wind deflection resulted in the creation of a crescent-shaped dune wrapping around the crater (Fig. 1) (McHone et al., 2002). As an obstacle to surface sand transport, a sand ramp built up over ejecta against the eastern crater rim and sand spills over in at least two places (O'Neill and Heine, 2005). The crater is partly infilled with dust, sand, and chemical precipitates associated with an ephemeral groundwater-window lake (Miller et al., 2018).

To create a 3D map of the crater's geomorphology, we used structure-from-motion photogrammetry. Photogrammetry provides a cost effective and rapid method of using aerial imagery to create three-dimensional models. To create the model, we used photography from a light aircraft taken obliquely across the crater from an elevation of 700-800 m (T. Brattstrom pers comm.). The photographs were georeferenced using Digitalglobe satellite imagery and the Shuttle Radar Topography Mission (SRTM) one arc-second digital elevation model (DEM) (~30 m at the equator) on the surrounding terrain. We estimate the resultant 1.5 m digital surface model (DSM) has a precision of less than 5 m. The accuracy of the underlying SRTM DEM is 7.2 m in the horizontal and 6 m in the vertical in Australia (Rodríguez et al., 2006).

The orthomosaic and DSM constructed from the aerial photography is presented in Figure 1. Measured from the model, the crater has a perimeter of 2,830 m and an area of 624,635 m^2. The maximum width is in a NE-SW direction of 946 m. The circularity index is >0.9, indicating the crater is very circular (Adler and Salisbury, 1969) and has a relatively uneroded crest. Assuming a circular shape, the average diameter is 892 m. The lowest point on the crater floor is 325 m a.s.l. and the highest point on the rim is 384 m on the north-western side, giving a total depth of 59 m and a maximum height of 33 m above the western plain at 351 m. This rim height is close to that predicted (~35 m) by the empirical relationship of (Melosh, 1989). The resultant depth/diameter ratio (0.07) is much less than for a fresh lunar crater, which tend to be parabolic (Mahanti et al., 2018), meaning there is significant infilling by sediments. A depth/diameter ratio of 0.2 (Pike, 1977) predicts a depth of 178 m, meaning it is possible that the crater contains ~120 m of fill. Given the well-preserved crater walls, this sediment must originate from outside the crater.

EXPOSURE DATING

Exposure dating with cosmogenic nuclides relies upon the assumption that a surface is instantaneously created by a geomorphological event that results in exposed rock surfaces that contain no inventory of cosmogenic nuclides. A desert environment is ideal for preservation of impact craters because of low erosion rates. However, low erosion rates result in high concentrations of cosmogenic nuclides in surface rocks, increasing the potential for inheritance. Large impact craters are suitable for dating where there is overturning of bedrock or ejection of underlying basement deeply buried prior to the impact. The geology surrounding Wolfe Creek Crater is a gently undulating bedrock surface dipping to the south at ~1 $m.km^{-1}$ (Miller et al., 2018) with a thin, discontinuous cover of laterite (Fudali, 1979). O'Neill and Heine (2005) observed variable amounts of overturn around the rim of Wolfe Creek crater. Average overturn is 100-110°, greatest in west-southwest at 130° and least in the east-northeast at 40-60° from horizontal. This pattern is consistent with the distribution of ejecta, shatter cones, and recovered meteorite fragments, which suggest the projectile came in from the east-northeast (O'Neill and Heine, 2005).

The southeast side of the crater was chosen because of prominent (>1 m high) outcrops of ejecta suitable for sampling. Four samples (WCC-01 to -04) were collected from relatively flat surfaces on the highest points of exposed quartzite above the surface along the crater rim (Fig. 1; Table 1). All samples consisted of Canning Basin Devonian quartzite. According to the geological map of Shoemaker et al. (2005), the sample sites are located in lower sandstone ejecta (WCC-01, 02) and upper sandstone ejecta (WCC-03, 04). Given that the height of the rim in these locations is ~20 m above in situ bedrock, it is very likely that these surfaces were formerly deeply buried under cover before the impact. For samples WCC-01, 02, the lower sandstone is >10 m below the

plain surface and for WCC-03, 04, the upper sandstone is >5-10 m below the surface according to the map of Shoemaker et al. (2005). An iron-rich weathering rind is present on the surface of exposed quartzite. On neighbouring surfaces that were broken, the weathering rind is not present. This quartz-rich rock is unlikely to erode rapidly. There was no evidence of broken material below outcrops that suggests that the surface is actively physically weathering. There is also no evidence of erosion of a former ejecta cover in the form of lag. Both vegetation cover and shielding of the horizon in this flat terrain is negligible.

Two of the samples (WCC-01 and WCC-04) were subdivided before crushing and run in duplicate. We extracted ^{10}Be and ^{26}Al from separated quartz using standard methods (e.g. Barrows et al. (2001)). Aluminium was measured using ICP-OES with a precision of <± 0.9% with no systematic error. Carrier of 255 μg of ^{9}Be made from deep-mined beryl was added to each sample. The isotopic ratios of ^{10}Be/Be and ^{26}Al/Al were measured by accelerator mass spectrometry on the 14UD accelerator at the Australian National University (Fifield et al., 1994). The ^{10}Be/Be ratio was measured relative to the NIST SRM 4325 standard (Table 1). The ^{26}Al/Al ratio was measured relative to a dilution of the ICN standard, cross-calibrated to that of KNSTD (Vogt et al., 1994) using a gas-filled magnet (Fifield et al., 2006). We use the default production rates for ^{10}Be and ^{26}Al from quartz from Borchers et al. (2016) and calculate ages using version 3 of the CRONUS calculator (Balco et al., 2008), normalised using the Nishiizumi et al. (2007) value for NIST SRM 4325. We scale the ages using the scheme of Lifton et al. (2014); LSDn). Statistical tests are based on internal uncertainties only but final exposure ages are also reported with external uncertainties from production rates in brackets. External uncertainties in conjunction with the LSDn scheme are ~6% for ^{10}Be and 9% for ^{26}Al. Mean ages are reported with an error which is the greater of the weighted mean error or the external error.

The exposure ages range from 86-128 ka (Table 2). It is very unlikely that the ages are from one statistical population where the error is likely to be due to random error (χ^2/ν =25.7). Agreement within error between duplicates (WCC-1, 04) indicates that the differences in age are inherent to the samples themselves. The ^{10}Be and ^{26}Al ages on each sample also agree within 1σ. The four ages for WCC-01 are consistent with a single population with an age of 120.4 ± 2.9 ka (χ^2/ν = 0.68) and similarly for WCC-04 (88.7 ± 2.6 ka; χ^2/ν = 0.34). The oldest samples (WCC-01, 03) have a mean exposure age of 120.0 ± 2.6 ka (χ^2/ν = 0.1), and the youngest (WCC-02, 04) have a mean exposure age of 87.7 ± 2.0 ka (χ^2/ν = 0.4).

Comparison of the age of Wolfe Creek crater with Meteor Crater is complicated by the fact that the exposure dating there was conducted at the inception of the technology (Nishiizumi et al., 1991). Standardisation, estimates of shielding, the half-life of ^{10}Be and scaling procedures have changed considerably since then. To make the comparison, we re-calculate the original exposure ages of Meteor Crater using the reported ^{10}Be and ^{26}Al data. Where data was not reported or was missing, we used other available sources. Latitude, longitude, horizons, and altitude were calculated using Fig. 1 in Nishiizumi and LiDAR data (Fig.3; Table 1). We assumed sample thickness was 1.5 cm, which is the maximum stated in the text. We assumed based on usage at the time that ^{10}Be samples were run against the Arnold-Nishiizumi ICN standard (A-N 3.77) (Middleton et al., 1993) and ^{26}Al samples against an NBS standard diluted at La Jolla, both assumed to be equivalent to KNSTD. Samples were collected in the sandy dolomite of the Kaibab Formation where the dry bulk density has been measured in cored material from the rim at 2.28 g.cm^{-3} (Watkins and Walters, 1966). No erosion or snow cover is assumed, so therefore the exposure ages are a minimum. Exposure ages were otherwise calculated as above.

The ^{10}Be and ^{26}Al data fall into distinct groups (Table 2). The four samples from the wall (M-1 to M-4) are systematically younger than the other samples, ranging from 20-33 ka, as noted by Nishiizumi et al. (1991). The seven ^{10}Be ages from the ejecta and the rim (M-5 to M-11) do not come from a single statistical population ($\chi^2/\nu = 198$). M-6 is heavily shielded by the boulder from which it was collected. Of the remaining 6 samples, 4 samples (M-5, 7, 10, 11) group together ($\chi^2/\nu = 1.6$) with a mean age of 62.7 ± 2.0 ka. In contrast, 5 of the ^{26}Al exposure ages (M-5, 7, 8, 10, 11) on the same 6 samples have similar scatter ($\chi^2/\nu = 1.7$) with a mean age of 59.4 ± 2.0 ka. .

OPTICAL DATING

Given that the crescent-shaped dune system adjoining Wolfe Creek Crater must have formed after the impact, we attempted to constrain the age of the crater by dating sediment within the dune. Optically stimulated luminescence (OSL) is an ideal technique for dating quartz-rich sandy landforms in a desert environment. Optical dating provides an estimate of the time elapsed since luminescent minerals were last exposed to sunlight (Huntley et al., 1985). Sand grains buried within a sandy deposit accumulate the effects of the radiation flux to which they are exposed, and the burial dose (equivalent dose, DE) can be measured using the optically stimulated luminescence (OSL) signal. Australian desert sand in particular is usually well bleached and sensitive (Fitzsimmons et al., 2010).

The northern arm of the deflected crescent dune is more strongly developed than the southern arm (Fig. 1). A site on the crest of the northern arm, 430 m northwest of the crater (Fig. 1) was selected for the augering of two holes (01WCC-13, 01WCC-14), one meter apart. Both holes were augered through dune sand and into a mixed ferricrete/sand layer at about 10 m depth (Fig. 3). Samples from the first hole (01WCC-13) were collected for magnetic susceptibility, grain

size and stable isotope analysis on organic matter (Miller et al., 2018). Samples for OSL were taken from the second hole (01WCC-14) at 5 depths in 25 cm long stainless steel tubes (Fig. 3). OSL samples were not collected below 833 cm because of the presence of ferricrete.

Miller et al. (2018) divided the stratigraphy of the dune into 4 units based on the magnetic susceptibility of the sediment and the clay content (Fig. 3). The lowest unit consists of a mixture of dune sand and ferricrete, and overlies a ferricrete thought to extend beyond the dune itself. The next three units are dune sand, the uppermost 5 m of the dune is ~98% sand size. The boundary between units 2 and 3 (7.2 m) is where clay content decreases below 5% and continues to decrease to near zero at the dune surface. The sedimentary change may indicate a change in environmental conditions or a change in the surface wind field. A surveyed cross-section reveals an asymmetry in the dune form, suggesting there may be an underlying sand plain that pre-dates the longitudinal dune (Miller et al., 2018). Based on the cross-profile, at least the upper 4 m is part of the crescent dune, and probably the upper 6 m (Miller et al., 2018). No obvious hiatuses were observed in the 10 m thickness.

The OSL methodology is described in Miller et al. (2018) and more complete methodological details are in Spooner et al. (2001). The samples are well bleached aeolian sediment lacking any visible evidence of post-depositional bioturbation or other mixing. Bulk sediment from the 8 m depth used for dating was analysed for U, Th and K concentrations, which were measured by neutron activation analysis and delayed neutron activation (NAA/DNA); K was calculated from measurements of K_2O by x-ray fluorescence (XRF). Radioisotope activities for U, Th, and K were also measured by high-resolution gamma spectrometry and subsequently converted to concentrations; these data confirmed secular equilibrium in the U and Th decay

chains. Cosmic ray dose rates were calculated following Prescott and Hutton (1994), making allowance for site altitude, geomagnetic latitude and time-averaged thickness of sediment overburden. Alpha-particle irradiation from radioisotopes within the etched quartz grains was assumed to be 10% of the external activity, and the efficiency with which alpha-particle irradiation induced OSL (a) was assumed to be 0.04 ± 0.01. Measured water content was assumed to be the long-term average.

In the laboratory, 90-125 μm quartz grains were isolated from each sediment sample under low-intensity red and orange light. OSL measurements were performed on approximately 5 to 6 mg of etched quartz attached by silicone oil to the central 7 mm diameter of each of 128 stainless steel discs. The OSL signal was measured on an Elsec Type 9010 automated reader with 500 ± 80 nm stimulation, and UV emissions detected by an EMI 9235QA photomultiplier tube optically filtered by one UG 11 and one U-340 filter and P determined by the "Australian slide" using a linear plus single saturating exponential fit (scale factor = 1.00). The advantage of multiple-grain OSL over single-grain OSL for these stratified low-dose-rate sediments is that the use of many grains effectively eliminates small-scale dose heterogeneity by averaging out the slight grain-to-grain differences in beta dose.

The optical ages are presented in Table 3. The three levels dated increase in age as expected for accumulating sand. Assuming that the sand at the base accumulated at a constant rate, the sedimentation rate is 6 cm/1000 yr between the lowest two ages. Using this rate, the sand/ferricrete contact at 9.96 m occurs at 137 ka. This represents a maximum age for dune formation, and therefore implicitly for the crater. Miller et al. (2018) argue that Unit 4, which contains large fragments of ferricrete cannot be of aeolian origin and more likely represents a sand-ferricrete

mixture thrown out by the impactor landing close to the crest of an extant longitudinal dune. The Unit 4/3 boundary is probably the base of aeolian sand deposition. This level has an interpolated age of 120 ka and is the most likely age for the formation of the crater derived from the dune disturbance. These ages must be considered approximate since sand units in dunes are likely to be deposited quickly, and in succession (e.g. Fitzsimmons et al. (2007)).

DISCUSSION

Crater morphology

Our new measurements of Wolfe Creek Crater improve upon the earlier estimates of Gottwald et al. (2017), Hawke (2003), and O'Neill and Heine (2005). The DSM reveals the broadest section of the flank is in the east (Figure 1). The banked-up sand in the east obscures the amount of ejecta on this side. Miller et al. (2018) found that this sand cover was a veneer and only ~3 m thick over ejecta. Miller et al. (2018) recovered 10 m of crater fill mostly of aeolian origin and found that fans from the walls consist only of slopewash from the walls. These observations are consistent with minimal erosion of the rim crest and the absence of a former ejecta covered which was removed by erosion. Fudali (1979) measured the regional gravity gradient across the crater to calculate an approximate total (minimum) depth of 140-150 m, which agrees well with the assumption of a parabolic shape. This estimate is a function of assumed bulk density of the crater and infill. This also assumes that the bottom third consisted of fall-back rubble, which is high compared to lunar craters. Hawke (2003) conducted an airborne geophysical survey and using the same density measurements agreed with the results of Fudali (1979); a thickness of 95 m of low-density crater fill, overlying 170 m of autochthonous breccia, giving apparent and true crater depths of 150 and 320 m respectively (Hawke, 2003). They concluded that most of the infill is

likely to be sand. However, O'Neill and Heine (2005) found a 4-layer model to be most consistent with their geophysical data, consisting of a ~10 m deep claypan, another 10 m of clay-rich sediment, overlying a breccia to 120 m and fractured bedrock to 200 m.

Impact crater age

Exposure dating provides a useful method of directly dating craters that have sufficient size to expose formerly deeply buried rock. Two factors limit the accuracy of exposure dating in these settings. The first is inheritance of exposure from the previous surface. Inheritance results in a maximum limiting age for the crater. The second factor is weathering (physical or chemical) of the crater rim or erosion of an ejecta sheet. This process results in a minimum limiting age for the cratering event. Observation of geomorphic processes, combined with the distribution of ages, is key to determining whether either or both these effects are operating. Nakamura et al. (2014) found that by not sampling outcrop at Lonar crater, the exposure ages had considerable scatter, almost certainly because of former shielding.

At Wolfe Creek crater, the OSL ages from the dune profile place the perturbation of the linear dune after 137 ka, and most likely at ~120 ka. An independent estimate of age comes from dated cored material in the crater floor. Miller dated oogonia from an equivalent of ~5 m depth in the crater fill at 13.4 ka. Applying the sedimentation rate from this sample, the upper 20 m fill suggested by O'Neill and Heine (2005) has a basal age of ~115 ka. The oldest OSL age of 28.6 ka from 6.6 m depth would place the basal age at ~87 ka, further supporting a young age for the crater. These ages must be used with caution because sedimentation rates are likely to be much higher in the deepest fill because of the steeper slopes at that time.

Two possible scenarios explain the exposure ages, either a younger (~ 89 ka) or an older exposure age (~120 ka). For a younger scenario, inheritance must affect the older exposure ages. For the older scenario, weathering of the sampled surface or removal of ejecta has resulted in the two younger exposure ages. Quartzite is highly resistant to weathering and is unlikely to erode at a rate higher than 1-2 m/Ma in a desert environment, comparable to rates observed on Australian desert granites (Bierman and Caffee, 2002). If the surface of the younger samples was eroding at a rate of 1-2 m/Ma, this would increase the exposure age by ~10-20% and likely account for most of the difference between the two age groups. Rim morphology is well preserved, and we found no evidence for removal of an ejecta sheet, but alluvial fans are actively transporting fines from the crater walls onto the crater floor. The OSL data, in conjunction with the sedimentary data, support an older age for the crater, since the dune owes its existence to deflection of the dune field. We consider the impact occurred at 120.0 ± 2.6 (9.1), which is the average of the means of the older ^{10}Be and ^{26}Al ages. This age may be a minimum if some weathering has occurred at these sample sites.

Shoemaker et al. (1990) calculated an age of ~300 ka based on unpublished ^{36}Cl/^{10}Be and ^{41}Ca/^{36}Cl ratios in a piece of meteorite found by Taylor (1965) some 4 km from the crater. Despite being relatively unweathered and unburied by sand and different material to that found at the crater, Buchwald (1975) believed it belonged to the same impact. Fresh meteoritic material is extremely rare at the crater and only 1.3 kg was collected in early studies (Cassidy (1954); McCall (1965); Knox, (1967)). The vast majority of meteoritic material recovered from the impact crater is in the form of iron-dominated impactite, with ‘shale balls’ up to 300 kg in weight, several thousand kg having been collected in total (McCall and De Laeter, 1967). This constitutes a sizeable fraction of the estimated ~14,000 t asteroid (O'Neill and Heine, 2005). Given the discrepancy with the

terrestrial age of the meteorite, it is unlikely that the dated fragment belonged to the Wolfe Creek meteorite. However, given that terrestrial exposure ages calculated for the Canyon Diablo meteorite from Meteor Crater are in some cases five times the measured impact age (Schnabel et al., 2001), it is still possible there is an association.

The weighted mean age of the combined Meteor crater ^{10}Be and ^{26}Al mean exposure ages is 61.1 ± 2.3(4.8) ka, ~20% older than previously reported (Nishiizumi et al., 1991). Insufficient data is presented to revise the exposure ages published by Phillips et al. (1991). However, unpublished data revises these ages to 56.0 ± 2.4 ka, within error of the ^{10}Be and ^{26}Al exposure age (Marrero et al., 2010; Marrero et al., 2016). Inheritance is not an issue in this setting because of the complete shielding of the Kaibab formation before impact, therefore the most likely age is the oldest. The samples from walls (M-1 to M-4) give apparent ages of 20-33 ka which probably relates to geomorphic instability on these steep slopes in the late Pleistocene (Nishiizumi et al., 1991). The similarity to the apparent ages of the walls at Wolfe Creek Crater probably indicates similar instability (Nishiizumi et al., 1991). Nishiizumi et al. (1991) present an argument for the erosion of ~8 m of ejecta based on a measurement (M6) from the flank of a boulder. However, self-shielding from the boulder is not described in the calculations making it difficult to verify the calculation.

The exposure age is ~20% older than an independent thermoluminescence (TL) age calculated on shocked quartz (Sutton, 1985). The TL ages range from 37.7 ± 4.2 to 53.6 ± 3.5 ka with mean ages for the two rock types analysed (sandstone and dolomite) of 50.4 ± 2.9 ka and 46.0 ± 3.1 ka respectively. An insufficient period of heating to completely reset the quartz is unlikely in this case because of the internal agreement between the samples. Sutton (1985) averaged 7 of

these ages to produce a mean age of 49.0 ± 3.0 ka and estimated that anomalous fading could account for a maximum effect of a 20% reduction of the age, but considered it to be unlikely. To assess the effect of anomalous fading, we regressed the ages against non-silica natural TL. This function predicts an age of 51.5 ± 3.7 ka where non-silica natural TL is zero, and is outside the uncertainty of the mean exposure age external error. Reassessment of this thermoluminescence age awaits the application of modern optical dating.

Impact cratering rate

The Australian continent has one of the best-preserved impact-cratering records on Earth (Haines, 2005). At least 30 impact structures have been identified in Australia and eight of these were formed during the Pleistocene. The oldest and largest of these is Darwin crater in Tasmania which is dated at 816 ± 7 ka using $^{40}Ar/^{39}Ar$ on Darwin glass (Lo et al., 2002). Exposure dating has been attempted on three of the smallest craters: Boxhole (~170 m), Henbury (~180 m) and Dalgaranga craters (24 m). Unpublished exposure ages on a quartz vein collected from low on the crater wall and for a quartz block in the ejecta deposit on the rim place Boxhole at ~30 ka (Shoemaker et al., 1990). Rocks at both Dalgaranga and Henbury had significant inheritance (Shoemaker et al., 1990). However, meteorite cosmogenic ^{14}C decay ages puts Boxhole at 5.4 ± 1.5 ka and Henbury at 4.2 ka ± 1.9 ka (Kohman and Goel, 1962). Shoemaker and Shoemaker (1988) suggested Dalgaranga crater may be younger than 3 ka and Veevers crater less than 4 ka. The degree of preservation of Snelling crater suggests an age of probably <5 ka (Glikson, 1996). The newly discovered Hickman crater (270 m) is undated but likely to be <100 ka (Glikson et al., 2008).

It is problematic calculating a cratering rate from terrestrial data. The Earth's atmosphere reduces the number of events through braking and ablation of meteors and atmospheric detonations (such as the Tunguska bolide). Most stony bodies <150 m do not reach the surface (Shoemaker, 1983). The cratering record beyond ~100 ka is incomplete because of the likelihood of rapid destruction of small craters on a geomorphically active planetary surface. Most (73.6%) of the Earth has no impact record, since 70.99% is ocean and 2.59% is ice sheet on Antarctica. Impactor sizes of <15 m are unlikely to produce tsunamis capable of leaving a geomorphic impact unless adjacent to a coast (Gisler et al., 2011). Many regions are re-surfacing, such as the major fluvial basins (the Murray and Eyre Basins in Australia), dunefields and the areas under the Pleistocene ice sheets and icefields. There is therefore a preservation bias to arid and semi-arid cratonic regions. A short time period is necessary to capture the preservation of small craters but because of the low frequency of large (>1 km) impacts it does not capture enough large events from which to make meaningful estimates for these larger events. However, the cratering rate for recent history cannot be estimated from extra-terrestrial bodies, such as the moon, because the craters there cannot be accurately dated and crater saturation equilibrium is widespread. Lastly, calculating a cratering rate by modelling impactors is a nontrivial task (Bland and Artemieva, 2006). Therefore, the last ~100 ka is a useful period for determining the rate of the small (<15 m), more frequent impactors capable of generating a significant crater (>25 m up to 1 km).

Australia provides an ideal area to determine a recent cratering rate because of good crater preservation due to aridity and little resurfacing, and the number of dated craters. However, because of erosion and incomplete mapping, there can only be a minimum estimate and we have to assume that this region is representative of the Earth as a whole. With the revision in age of Wolfe Creek Crater, there have been 7 identified impacts producing craters >25 m (probably only

iron meteorites) in diameter in the last ~120 ka. This interval contains the best dated impact craters and the number of craters older than this drops off rapidly, probably because of preservation. This is a rate of 1 crater per 17,000 years. Given that the crater count is confined to the semi-arid/arid zone of Australia (~70% of its area) and Australia is ~1.5% of the Earth's surface, the rate is one impact capable of producing a crater every ~180 years. This is equivalent to a rate of 11×10^{-6} km^{-2} 10^{-6} yr^{-1} ($=11 \times 10^{-12}$ km^{-2} yr^{-1}). The estimated rate for terrestrial craters >20 km in diameter from North America and Europe for the last 120 Ma (Shoemaker and Shoemaker, 1998) is 5.6 ± 2.8 10^{-15} km^{-2} yr^{-1}. This is similar to the rate of 5.3 ± 1.8 10^{-15} km^{-2} yr^{-1} estimated for the Copernican era (0.8-0 Ga) on the moon (Shoemaker and Shoemaker, 1998). Our measured rate for small impactors is about 2000 times higher than these rates, reflecting their much higher abundance. Stony objects generally fragment much more, the fragments are much smaller, and these fragments have lower impact velocities (Bland and Artemieva, 2006), resulting in far fewer craters. If 5% of meteors are iron (Bland and Artemieva, 2006; Shoemaker, 1983), the rate for all meteors including those that do not survive the atmosphere may be 20 times higher than the rate calculated above because of the low cratering efficiency of stony objects (Bland and Artemieva, 2006).

The cratering rate for small craters on Australia provides a baseline from which to compare simulations of impact frequency on Earth and to assess the completeness of the geomorphological record. Bland calculated that over a 100,000 period, 180–200 craters >0.1 km, 60–70 >0.15 km, 8–10 >0.3 km and 4 >0.5 km would be expected. Bland and Artemieva (2006) estimated that the frequency of a Wolfe Creek size impactor on the Earth is one every 13,000 years and a Henbury-like event (crater fields with largest craters ~0.16 km) every 500 years. Although the record is more complete at large crater size, either a large number of craters of smaller size await discovery (Hergarten and Kenkmann, 2015) or they have not been preserved. The presence of large areas of

dune field in central Australia has probably obscured the smallest craters and some may be buried within fluvial or lacustrine deposits. The preservation potential in these active environments is also low. It is difficult to estimate the error involved in our cratering rate. Our estimate is based on small numbers and a relatively short period of geological time. Because of the limitations outlined above including a lack of high-quality dating, our rate is likely to be only a minimum estimate of the terrestrial cratering rate for small objects.

ACKNOWLEDGEMENTS

The Aboriginal elders in Billiluna are thanked for permission to conduct our research in and around Wolfe Creek Crater and assistance with field work. The Department of Conservation and Land Management is thanked for technical permits for research in and around the crater in 2001. We thank Ted Brattstrom (Ka'u High School, Hawaii) for providing aerial photography which was invaluable for this project. Funding for the fieldwork at Wolfe Creek Crater was provided by US NSF (AGS-082254), Australian Research Council grant A00104515, and the Australian National University. We thank Editor in Chief Timothy Jull and two anonymous reviewers for helpful comments.

REFERENCES

Adler J. E. M. and Salisbury J. W. (1969) Circularity of lunar craters. *Icarus* **10**(1), 37-52.

Balco G., Stone J. O., Lifton N. A., and Dunai T. J. (2008) A complete and easily accessible means of calculating surface exposure ages or erosion rates from 10Be and 26Al measurements. *Quaternary Geochronology* **3**(3), 174-195.

Barrows T. T., Stone J. O., Fifield L. K., and Cresswell R. G. (2001) Late Pleistocene Glaciation of the Kosciuszko Massif, Snowy Mountains, Australia. *Quaternary Research* **55**(2), 179-189.

Bierman P. R. and Caffee M. (2002) Cosmogenic exposure and erosion history of Australian bedrock landforms. *Geological Society of America Bulletin* **114**(7), 787-803.

Bland P. A. and Artemieva N. A. (2006) The rate of small impacts on Earth. *Meteoritics & Planetary Science* **41**(4), 607-631.

Borchers B., Marrero S., Balco G., Caffee M., Goehring B., Lifton N., Nishiizumi K., Phillips F., Schaefer J., and Stone J. (2016) Geological calibration of spallation production rates in the CRONUS-Earth project. *Quaternary Geochronology* **31**, 188-198.

Buchwald V. F. (1975) *Handbook of Iron Meteorites*. University of California Press, Los Angeles.

Cassidy W. A. (1954) The Wolf Creek, Western Australia, meteorite crater. *Meteoritics* **1**, 197-199.

Fifield L. K., Allan G. L., Stone J. O., and Ophel T. R. (1994) The ANU AMS system and research program. *Nuclear instruments and Methods* **92**, 85-88.

Fifield L. K., Tims S. G., Gladkis L. G., Morton C. R., and Barrows T. T. (2006) Aluminium-26 measurements with beryllium-10 counting statistics. *Geochimica et Cosmochimica Acta* **70**(18, Supplement), A172.

Fitzsimmons K. E., Rhodes E. J., and Barrows T. T. (2010) OSL dating of southeast Australian quartz: A preliminary assessment of luminescence characteristics and behaviour. *Quaternary Geochronology* **5**(2-3), 91-95.

Fitzsimmons K. E., Rhodes E. J., Magee J. W., and Barrows T. T. (2007) The timing of linear dune activity in the Strzelecki and Tirari Deserts, Australia. *Quaternary Science Reviews* **26**(19-21), 2598-2616.

Fudali R. F. (1979) Gravity Investigation of Wolf Creek Crater, Western Australia. *The Journal of Geology* **87**(1), 55-67.

Gisler G., Weaver R., and Gittings M. (2011) Calculations of Asteroid Impacts into Deep and Shallow Water. *Pure and Applied Geophysics* **168**(6), 1187-1198.

Glikson A. Y. (1996) A compendium of Australian impact structures, possible impact structures, and ejecta occurrences. *AGSO Journal of Australian Geology & Geophysics* **16**, 373–375.

Glikson A. Y., Hickman A. H., and Vickers J. (2008) Hickman Crater, Ophthalmia Range, Western Australia: evidence supporting a meteorite impact origin. *Australian Journal of Earth Sciences* **55**(8), 1107-1117.

Gottwald M., Fritz T., Breit H., Schättler B., and Harris A. (2017) Remote sensing of terrestrial impact craters: The TanDEM-X digital elevation model. *Meteoritics & Planetary Science* **52**(7), 1412-1427.

Haines P. W. (2005) Impact cratering and distal ejecta: the Australian record. *Australian Journal of Earth Sciences* **52**(4-5), 481-507.

Hawke P. J. (2003) Geophysical investigation of the Wolfe Creek Meteorite Crater. In *Geological Survey of Western Australian Record*, pp. 9.

Hergarten S. and Kenkmann T. (2015) The number of impact craters on Earth: Any room for further discoveries? *Earth and Planetary Science Letters* **425**, 187-192.

Huntley, D.J., Godfrey-Smith, D.I., Thewalt, M.L.W., 1985. Optical dating of sediments. Nature 313, 105-107.

Knox R., Jr. (1967) Surviving Metal in Meteoritic Iron Oxide from the Wolf Creek, Western Australia, Meteorite Crater *Meteoritics* **3**(4), 235.

Kohman T. and Goel P. (1962) Terrestrial ages of meteorites from cosmogenic C14. In *Radioactive Dating*, pp. 395-411. International Atomic Energy Agency, Athens.

LaPaz L. (1954) Meteoritic material from Wolf Creek, Western Australia, Crater. *Meteoritics* **1**(2), 200-203.

Lifton N., Sato T., and Dunai T. J. (2014) Scaling in situ cosmogenic nuclide production rates using analytical approximations to atmospheric cosmic-ray fluxes. *Earth and Planetary Science Letters* **386**, 149-160.

Lo C.-H., Howard K. T., Chung S.-L., and Meffre S. (2002) Laser fusion argon-40/argon-39 ages of Darwin impact glass. *Meteoritics & Planetary Science* **37**(11), 1555-1562.

Mahanti P., Robinson M. S., Thompson T. J., and Henriksen M. R. (2018) Small lunar craters at the Apollo 16 and 17 landing sites - morphology and degradation. *Icarus* **299**, 475-501.

Marrero S., Phillips F. M., Caffee M. W., Smith S. S., and Kring D. A. (2010) Re-Dating the Barringer Meteorite Crater (AZ) Impact Using the Cosmogenic Chlorine-36 Surface Exposure Method. *Meteoritics and Planetary Science Supplement*, 5150.

Marrero S. M., Phillips F. M., Borchers B., Lifton N., Aumer R., and Balco G. (2016) Cosmogenic nuclide systematics and the CRONUScalc program. *Quaternary Geochronology* **31**, 160-187.

McCall G. J. H. (1965) Possible meteorite craters – Wolf Creek, Australia and analogs. *Annals of the New York Academy of Sciences* **123**(2), 970-998.

McCall G. J. H. and De Laeter J. R. (1967) Catalogue of Western Australian meteorite collections. *Special publication (Western Australian Museum)* **3**.

McHone J. F., Greeley R., Williams K. K., Blumberg D. G., and Kuzmin R. O. (2002) Space shuttle observations of terrestrial impact structures using SIR-C and X-SAR radars. *Meteoritics & Planetary Science* **37**(3), 407-420.

McNamara K. (1982) *Wolf Creek Crater*. Western Australia Museum, Perth. pp. 16.

Melosh H. J. (1989) *Impact Cratering. A Geologic Process*. Oxford University Press, Oxford.

Middleton R., Brown L., Dezfouly-Arjomandy B., and Klein J. (1993) On 10Be standards and the half-life of 10Be. *Nuclear Instruments and Methods in Physics Research Section B: Beam Interactions with Materials and Atoms* **82**(3), 399-403.

Miller G. H., Magee J. W., Fogel M. L., Wooller M. J., Hesse P. P., Spooner N. A., Johnson B. J., and Wallis L. (2018) Wolfe Creek Crater: A continuous sediment fill in the Australian Arid Zone records changes in monsoon strength through the Late Quaternary. *Quaternary Science Reviews* **199**, 108-125.

Nakamura A., Yokoyama Y., Sekine Y., Goto K., Komatsu G., Kumar P. S., Matsuzaki H., Kaneoka I., and Matsui T. (2014) Formation and geomorphologic history of the Lonar impact crater deduced from in situ cosmogenic 10Be and 26Al. *Geochemistry, Geophysics, Geosystems* **15**(8), 3190-3197.

Nishiizumi K., Imamura M., Caffee M. W., Southon J. R., Finkel R. C., and McAninch J. (2007) Absolute calibration of 10Be AMS standards. *Nuclear Instruments and Methods in Physics Research Section B: Beam Interactions with Materials and Atoms* **258**(2), 403-413.

Nishiizumi K., Kohl C. P., Shoemaker E. M., Arnold J. R., Klein J., Fink D., and Middleton R. (1991) *In situ* ^{10}Be-^{26}Al exposure ages at Meteor Crater, Arizona. *Geochimica et Cosmochimica Acta* **55**(9), 2699-2703.

O'Neill C. and Heine C. (2005) Reconstructing the Wolfe Creek meteorite impact: deep structure of the crater and effects on target rock. *Australian Journal of Earth Sciences: An International Geoscience Journal of the Geological Society of Australia* **52**(4), 699 - 709.

Phillips F. M., Zreda M. G., Smith S. S., Elmore D., Kubik P. W., Dorn R. I., and Roddy D. J. (1991) Age and geomorphic history of Meteor Crater, Arizona, from cosmogenic 36Cl and 14C in rock varnish. *Geochimica et Cosmochimica Acta* **55**(9), 2695-2698.

Pike R. J. (1977) Apparent Depth/Apparent Diameter relation for Lunar Craters. *Proceedings of the 8th Lunar and Planetary Science Conference* 3427-3436.

Prescott J. R. and Hutton J. T. (1994) Cosmic ray contributions to dose rates for luminescence and ESR dating: Large depths and long-term time variations. *Radiation Measurements* **23**(2), 497-500.

Rodríguez E., Morris C. S., and Belz J. E. (2006) A Global Assessment of the SRTM Performance. *Photogrammetric Engineering & Remote Sensing* **72**(3), 249-260.

Schnabel C., Ma P., Herzog G. F., di Tada M. L., Hausladen P. A., and Fifield L. K. (2001) Terrestrial Ages of Canyon Diablo Meteorites. *Meteoritics & Planetary Science* **36**(Supplement), A184.

Scott E. R. D., Wasson J. T., and Buchwald V. F. (1973) The chemical classification of iron meteorites--VII. A reinvestigation of irons with Ge concentrations between 25 and 80 ppm. *Geochimica et Cosmochimica Acta* **37**(8), 1957-1976, IN1, 1977-1983.

Shoemaker E. M. (1983) Asteroid and Comet Bombardment of the Earth. *Annual Review of Earth and Planetary Sciences* **11**(1), 461-494.

Shoemaker E. M., Macdonald F. A., and Shoemaker C. S. (2005) Geology of five small Australian impact craters. *Australian Journal of Earth Sciences: An International Geoscience Journal of the Geological Society of Australia* **52**(4), 529 - 544.

Shoemaker E. M. and Shoemaker C. S. (1988) Impact Structures of Australia. In *Abstracts of the Lunar and Planetary Science Conference*, pp. 1079-1080.

Shoemaker E. M. and Shoemaker C. S. (1998) Impact cratering through geologic time. *Journal of the Royal Astronomical Society of Canada* **92**(6), 297-309.

Shoemaker E. M., Shoemaker C. S., Nishiizumi K., Kohl C. P., Arnold J. R., Klein J., Fink D., Middleton R., Kubik P. W., and Sharma P. (1990) Ages of Australian meteorite craters-a preliminary report. *Meteoritics* **25**, 409.

Spooner N. A., Olley J. M., Questiaux D. G., and Chen X. Y. (2001) Optical dating of an aeolian deposit on the Murrumbidgee floodplain. *Quaternary Science Reviews* **20**(5), 835-840.

Sutton S. R. (1985) Thermoluminescence measurements on shock-metamorphosed sandstone and dolomite from meteor crater, Arizona. 2. Thermoluminescence age of meteor crater. *Journal of Geophysical Research* **90**(B5), 3690-3700.

Taylor S. R. (1965) The Wolf Creek Iron Meteorite. *Nature* **208**, 944.

Vogt S., Wang M. S., Li R., and Lipschutz M. (1994) Chemistry operations at Purdue's accelerator mass spectrometry facility. *Nuclear Instruments and Methods in Physics Research Section B: Beam Interactions with Materials and Atoms* **92**(1), 153-157.

Watkins J. S. and Walters L. A. (1966) Laboratory physical property measurements on core and surface samples from six lunar analog test sites. In *Investigation of in situ physical properties of surface and subsurface site materials by engineering geophysical techniques project - Annual Report, fiscal year 1966* (ed. J. S. Watkins), pp. 317. U. S. Geological Survey.

FIGURES

Figure 1

Orthophoto and DEM of Wolfe Creek Crater showing sample dune core sites. Note the dunefield. Dashed lines indicate the shape of the crescent dune. Bumps to the north and west of the crater are trees. Map is projected in WGS84 UTM zone 52S.

Figure 2

Meteor Crater LiDAR map with sample sites. Map is projected in WGS84 UTM zone 12N.

Figure 3

Grain size data, sedimentary log and OSL ages of core 01WCC-13.

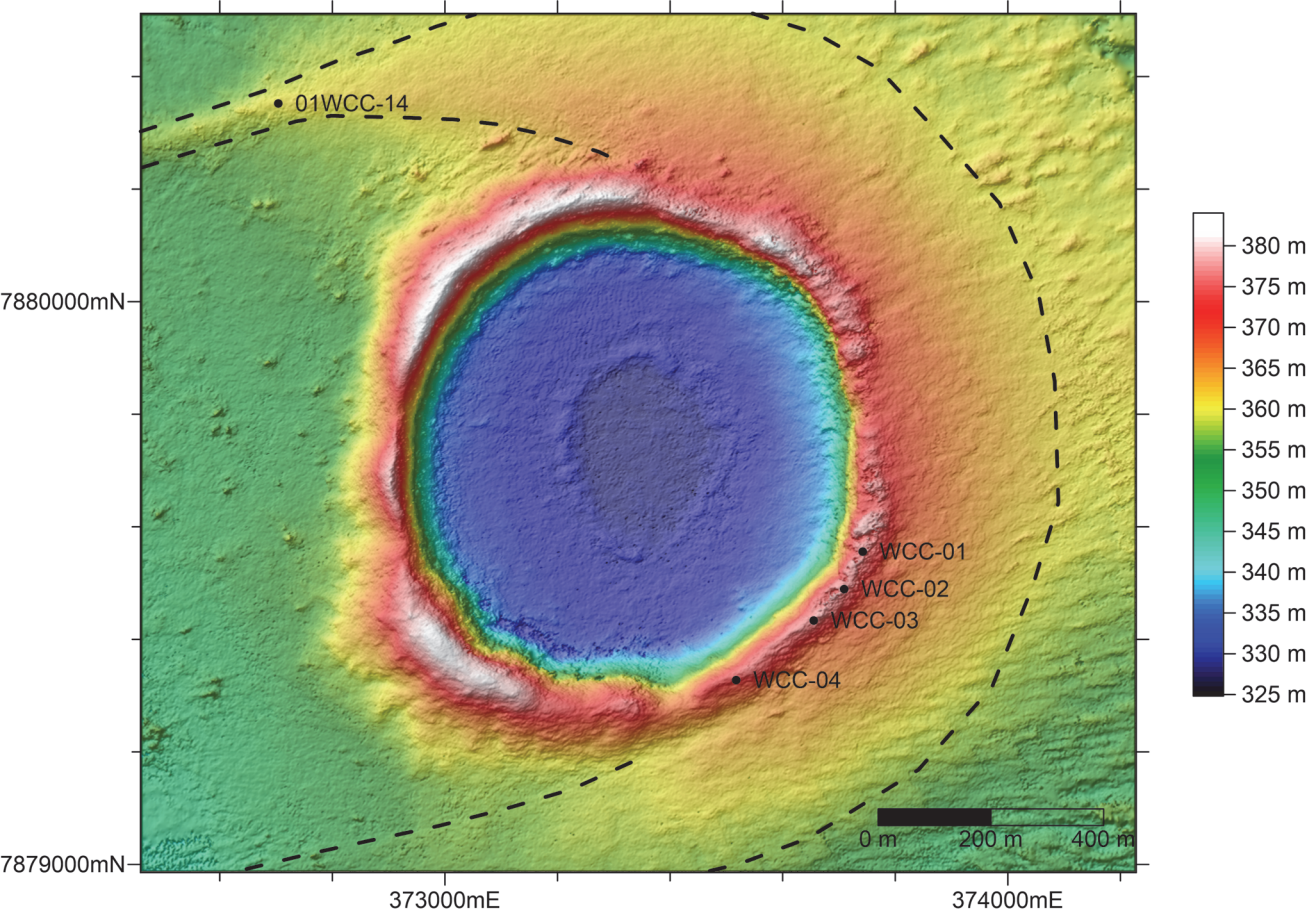
01WCC-14
WCC-01
WCC-02
WCC-03
WCC-04
7880000mN
7879000mN
373000mE
374000mE
0 m
200 m
400 m
380 m
375 m
370 m
365 m
360 m
355 m
350 m
345 m
340 m
335 m
330 m
325 m

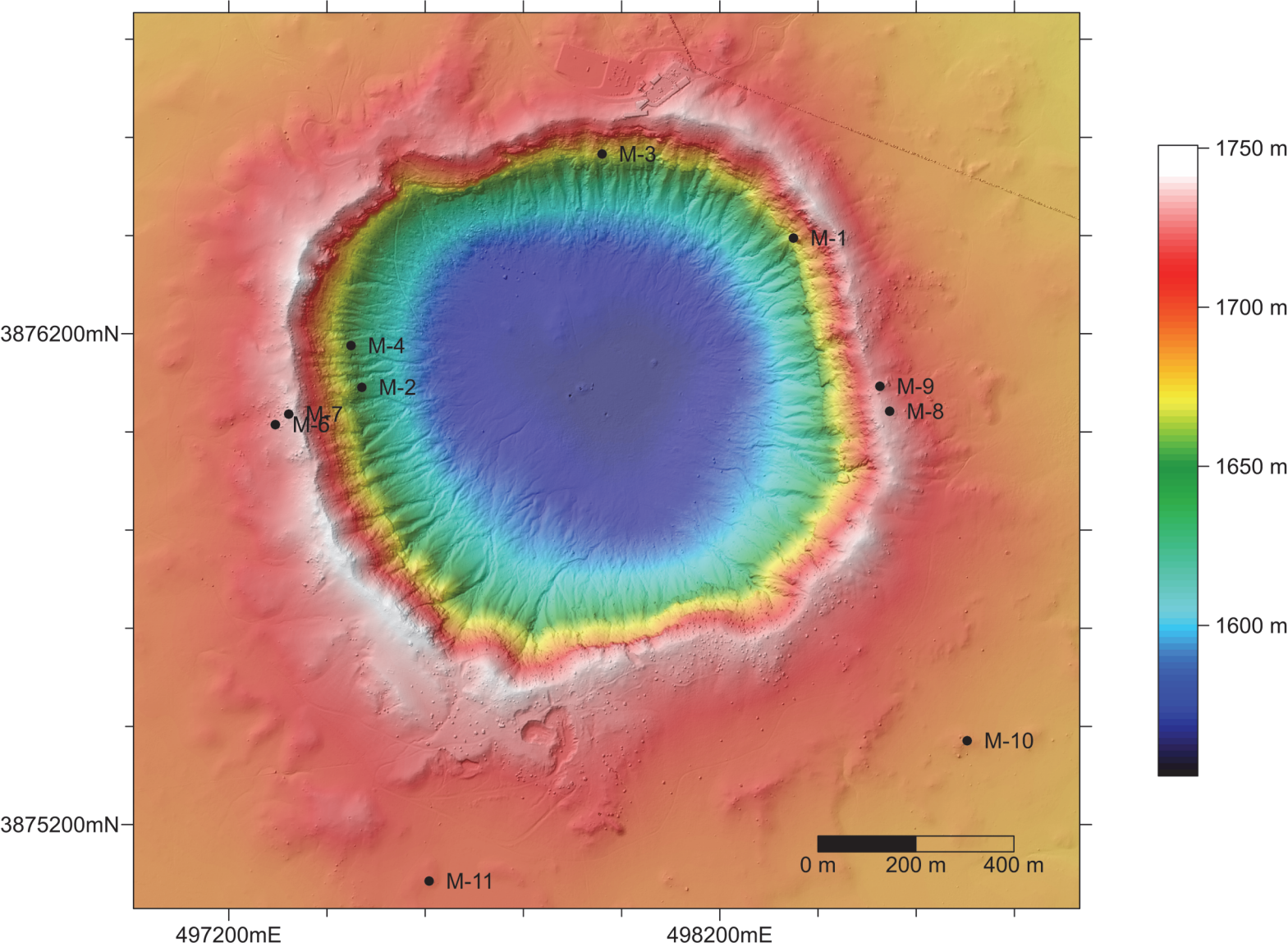
M-3
M-1
M-4
M-2
M-7
M-6
M-9
M-8
M-10
M-11
3876200mN
3875200mN
497200mE
498200mE
0 m
200 m
400 m
1750 m
1700 m
1650 m
1600 m

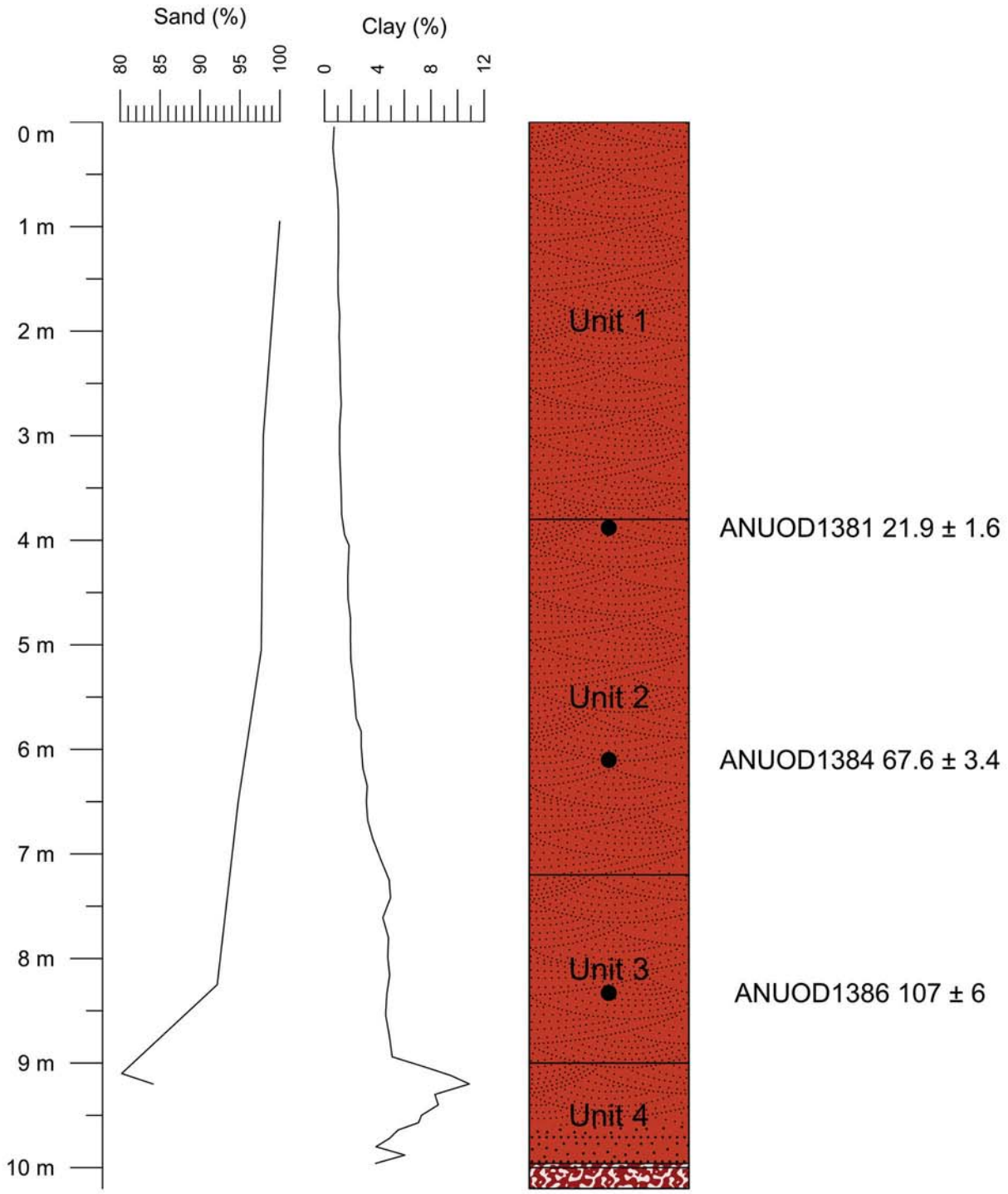
Sand (%)
80
85
90
95
100
Clay (%)
0
4
8
12
0 m
1 m
2 m
3 m
4 m
5 m
6 m
7 m
8 m
9 m
10 m
Unit 1
Unit 2
Unit 3
Unit 4
ANUOD1381 21.9 ± 1.6
ANUOD1384 67.6 ± 3.4
ANUOD1386 107 ± 6

TABLES

Table 1. Site data

Sample	Longitude (°E)	Latitude (°N)	Elevation (m)	Horizon correction	Thickness (cm)[1]
Wolf Creek Crater					
WCC-01(A/B)	127.7992	-19.1734	376	1.0	5/3.5
WCC-02	127.7989	-19.1740	377	1.0	5.0
WCC-03	127.7984	-19.1745	377	1.0	4.0
WCC-04(A/B)	127.7971	-19.1754	373	1.0	5.0/5.0
Meteor Crater					
M-1	-111.0181	35.0302	1678	0.9759	1.5
M-2	-111.0277	35.0275	1646	0.9860	1.5
M-3	-111.0224	35.0318	1675	0.9805	1.5
M-4	-111.0280	35.0282	1650	0.9770	1.5
M-5	-111.0297	35.0268	1738	1	1.5
M-6	-111.0297	35.0268	1730	1	1.5
M-7	-111.0294	35.0270	1738	1	1.5
M-8	-111.0159	35.0270	1732	1	1.5
M-9	-111.0162	35.0275	1732	1	1.5
M-10	-111.0142	35.0210	1695	1	1.5
M-11	-111.0262	35.0184	1705	1	1.5

1. Λ = 160 g.cm^{-2}, WCC ρ = 2.27 g.cm^{-3} (Fudali, 1979), MC ρ = 2.28 g.cm^{-3} (Watkins and Walters, 1966). (Nishiizumi et al., 1991) does not report individual depth measurements.

Table 2. Exposure ages

Sample	^{10}Be Lab code	[^{10}Be] (10^5 atoms g^{-1})[1]	Exposure age (yr)[2]	^{26}Al Lab code	[^{26}Al] (10^6 atoms g^{-1})[1]	[^{27}Al] (ug/g)	Exposure age (yr)[2]
Wolfe Creek Crater							
WCC-01A	ANU-M347-16	4.48 ± 0.17	117000 ± 4600	ANU-M364-05	3.06 ± 0.18	121.4 ± 1.1	128400 ± 8100
WCC-01B	ANU-M347-17	4.67 ± 0.18	120400 ± 4800	ANU-M364-06	2.96 ± 0.19	124.6 ± 1.1	123000 ± 8400
WCC-01 (mean)			118600 ± 3300				125700 ± 5600
WCC-02	ANU-M347-18	3.18 ± 0.12	86000 ± 3300	ANU-M364-07	2.24 ± 0.14	125.6 ± 1.1	96600 ± 6300
WCC-03	ANU-M392-14	4.61 ± 0.22	118600 ± 5800				
WCC-04A	ANU-M347-19	3.17 ± 0.15	86000 ± 4200	ANU-M364-08	2.17 ± 0.27	174.7 ± 1.6	94100 ± 12300
WCC-04B	ANU-M347-20	3.32 ± 0.13	90000 ± 3600	ANU-M364-09	2.06 ± 0.22	145.4 ± 1.2	89700 ± 10000
WCC-04 (mean)			88300 ± 2800				91700 ± 5700
Meteor Crater							
M-1		4.48 ± 0.31	32400 ± 2300		2.74 ± 0.22		32600 ± 2700
M-2		4.36 ± 0.37	32000 ± 2700		2.47 ± 0.20		30000 ± 2500
M-3		2.53 ± 0.31	19100 ± 2300		1.80 ± 0.15		22100 ± 1900
M-4		2.55 ± 0.32	19600 ± 2500		1.60 ± 0.14		20200 ± 1800
M-5		9.21 ± 0.51	60700 ± 3400		5.71 ± 0.52		62400 ± 5900
M-6		3.06 ± 0.13	21500 ± 900		1.68 ± 0.10		19500 ± 1200
M-7		8.33 ± 0.53	54400 ± 3500		5.60 ± 0.38		61200 ± 4300
M-8		6.87 ± 0.74	44400 ± 4800		4.97 ± 0.20		53900 ± 2200

M-9	5.43 ± 0.20	36300 ± 1300	3.63 ± 0.19	39400 ± 2100
M-10	8.42 ± 0.28	57200 ± 1900	5.73 ± 0.35	64700 ± 4100
M-11	9.40 ± 0.31	63500 ± 2100	5.00 ± 0.29	55600 ± 3300

1. WCC data are normalised to the NIST standard (2.79 x 10^{-11} $^{10}Be/^{9}Be$) and the Vogt standard (4.11 x 10^{-11} $^{26}Al/Al$). AMS measurements include additional 3% uncertainty on the standard. Carrier $^{10}Be/Be = 0.5 \times 10^{-16}$. Carrier ^{27}Al = 29 ± 10 ug; ^{26}Al Blank = 1.02 ± 0.22 x 10^{5} atoms. MC concentration data are from (Nishiizumi et al., 1991) and are normalised to KNSTD.

2. Error does not include external uncertainty for production rates.

Table 3. Optical ages

Lab code	ANUOD1381	ANUOD1384	ANUOD1386
Sample burial depth (m)	3.78-3.98	6.00-6.20	8.23-8.43
Palaeodose (Gy)	17.22 ± 0.54	72 ± 1.73	145.2 ± 5.7
Quartz grain diameter (μm)	107.5 ± 17.5	107.5 ± 17.5	107.5 ± 17.5
In situ water content (%)	1.87 ± 0.09	2.35 ± 0.12	3.29 ± 0.16
Saturation water content (%)	23 ± 2.3	21 ± 2.1	19 ± 1.9
In situ fraction of saturation	0.081 ± 0.01	0.112 ± 0.01	0.173 ± 0.02
NAA/DNA			
U (ppm)	0.57 ± 0.12	1.14 ± 0.148	1.17 ± 0.152
Th (ppm)	3.43 ± 0.086	4.7 ± 0.103	6.16 ± 0.123
K (%)	0.228 ± 0.036	0.223 ± 0.037	0.562 ± 0.053
Flame photometry			
K (%)	NA ± NA	0.32 ± 0.0128	0.52 ± 0.0208
Weighted mean			
U (ppm)	0.57 ± 0.12	1.14 ± 0.1482	1.17 ± 0.1521
Th (ppm)	3.43 ± 0.086	4.7 ± 0.1034	6.16 ± 0.1232
K (%)	0.228 ± 0.036	0.309 ± 0.0123	0.526 ± 0.0195
Cosmic ray dose-rate (Gy/ka)	0.16 ± 0.025	0.125 ± 0.02	0.1 ± 0.02
Total dose rate (Gy/ka)	0.785 ± 0.053	1.065 ± 0.047	1.354 ± 0.05
Age (ka)	21.9 ± 1.6	67.6 ± 3.4	107 ± 6

Notes: Growth curves were fitted using sat expon + lin, with scaling factor = 1; Alpha particle efficiency assumed to be 0.043 ± 0.01